AGU PUBLICATIONS

Geophysical Research Letters

RESEARCH LETTER
10.1002/2015GL065267

Special Section:
First Results from the MAVEN Mission to Mars

The first in situ electron temperature and density measurements of the Martian nightside ionosphere

C. M. Fowler[1], L. Andersson[1], R. E. Ergun[1], M. Morooka[1], G. Delory[2], D. J. Andrews[3], Robert J. Lillis[2], T. McEnulty[1], T. D. Weber[1], T. M. Chamandy[1], A. I. Eriksson[3], D. L. Mitchell[2], C. Mazelle[4,5], and B. M. Jakosky[1]

[1]Laboratory of Atmospheric and Space Sciences, University of Colorado Boulder, Boulder, Colorado, USA, [2]Space Sciences Laboratory, University of California, Berkeley, California, USA, [3]Swedish Institute for Space Physics, Uppsala, Sweden, [4]CNRS, Institut de Recherche en Astrophysique et Planétologie, Toulouse, France, [5]Institut de Recherche en Astrophysique et Planétologie, University Paul Sabatier, Toulouse, France

Key Points:
- First in situ nightside electron density and temperature profiles on the nightside of Mars
- Electron temperatures approach neutral atmospheric temperatures below 200 km
- Electron densities below 200 km require additional ionization source

Correspondence to:
C. M. Fowler,
christopher.fowler@lasp.colorado.edu

Citation:
Fowler, C. M., et al. (2015), The first in situ electron temperature and density measurements of the Martian nightside ionosphere, *Geophys. Res. Lett.*, *42*, doi:10.1002/2015GL065267.

Received 7 JUL 2015
Accepted 2 AUG 2015

Abstract The first in situ nightside electron density and temperature profiles at Mars are presented as functions of altitude and local time (LT) from the Langmuir Probe and Waves (LPW) instrument on board the Mars Atmosphere and Volatile EvolutioN (MAVEN) mission spacecraft. LPW is able to measure densities as low as ~100 cm^{-3}, a factor of up to 10 or greater improvement over previous measurements. Above 200 km, near-vertical density profiles of a few hundred cubic centimeters were observed for almost all nightside LT, with the lowest densities and highest temperatures observed postmidnight. Density peaks of a few thousand cubic centimeters were observed below 200 km at all nightside LT. The lowest temperatures were observed below 180 km and approach the neutral atmospheric temperature. One-dimensional modeling demonstrates that precipitating electrons were able to sustain the observed nightside ionospheric densities below 200 km.

1. Introduction

The dayside ionosphere of Mars is primarily the product of photoionization of the dayside neutral atmosphere by solar EUV radiation that undergoes a complex set of photochemical reactions. Its shape, structure, and solar zenith angle (SZA) dependence are well described by a classical Chapman profile at low altitudes [*Chapman*, 1931a], [*Chapman*, 1931b]. Comprehensive reviews of the Martian dayside ionosphere can be found in, for example, *Nagy et al.* [2004], *Witasse et al.* [2008], and *Withers* [2009].

In contrast, the nightside ionosphere of Mars is less well understood. Radio occultations of the nightside ionosphere were made by the Mars, Mariner, and Viking spacecraft in the 1960s, 1970s, and 1980s [see, for example, *Fjeldbo et al.*, 1970; *Savich and Samovol*, 1976; *Lindal et al.*, 1979]. *Zhang et al.* [1990] used this data set and found that around 60% of the radio occultation profiles between SZA 90° and 125° showed no detectable peak in electron density. The peaks that were observed typically lay between altitudes of ~140 and 180 km with densities of $\sim 5 \times 10^3$ cm^{-3}. It turns out that the nightside ionospheric densities were often too small to be detected by the radio occultation method. Due to the relative orbital geometries of Earth and Mars, radio occultations for SZA greater than ~125° were not possible.

More recently, *Němec et al.* [2010] analyzed 4 years of nightside ionospheric data from the Mars Advanced Radar for Subsurface and Ionospheric Sounding (MARSIS) instrument on board the Mars Express spacecraft. Their data set consisted of ~ 30,500 ionograms, observed at SZA >107° and altitude <1100 km. They identified ionospheric echoes in ~9% of these data, with peak densities less than 2×10^4 cm^{-3} and a lower limit to the peak altitudes of 100–150 km. Given that the lowest sensitivity of the MARSIS instrument is $\sim 5 \times 10^3$ cm^{-3}, they were able to estimate that ~90% of actual ionospheric density peaks (across all altitudes) are below this value. These ionograms were analyzed with respect to crustal magnetic field strengths, and it was found that in weak crustal field regions ($B < 20$ nT) the occurrence rate of the nightside ionosphere decreased with increasing SZA, up to ~125°. They suggest that dayside plasma transport plays a crucial role for ionospheric formation in these regions. For strong crustal field regions ($B > 20$ nT) they found no SZA dependence but rather a dependence on magnetic field orientation relative to the surface. The nightside ionospheric

occurrence rate was more than 4 times greater for near vertically aligned magnetic fields compared with horizontally aligned magnetic fields, suggesting the precipitating electrons (which can only enter the atmosphere when the magnetic field orientation allows it) could be a key ionization source for these regions.

With regard to modeling the nightside ionosphere and determining its source, several suggestions have been put forth. *Verigin et al.* [1991] used magnetotail data from the HARP electron spectrometer on board the Phobos 2 orbiter to investigate the effect of possible precipitating electrons. They showed that peak electron densities of a few thousand cubic centimeters, in agreement with previous observations of the nightside ionosphere, can be produced by the characteristic fluxes ($\sim 10^8$ cm^{-2} s^{-1}) and energies (tens of eV) observed by the instrument. *Haider et al.* [1992] extended this work using HARP electron spectra from the magnetotail and plasma sheet and drew similar conclusions.

Fox [1993] modeled upper limits to the nightside ionosphere using both precipitating electrons (based on the HARP data) and a dayside transport model. They computed electron density peaks in the range $\sim 1.5 \times 10^4$ cm^{-3} at altitudes of 159 to 179 km.

Haider [1997] used an analytical yield spectrum approach to model the chemistry of the major ions in Mars' nightside ionosphere. It was determined that the nightside ionosphere produced by precipitating magnetotail electrons agreed with Viking observations. Other sources of nightside ionization, such as plasma precipitation or horizontal plasma transport from the dayside, did not agree with the Viking profiles.

More recent modeling efforts by *Lillis et al.* [2009, 2011] used a Monte Carlo approach to calculate the electron impact ionization rates in the nightside Martian ionosphere as functions of energy spectrum, pitch angle distribution (PAD) of precipitating electrons, magnetic field magnitude, and neutral density. They found that inclusion of the magnetic field gradients and PADs are essential in obtaining correct ionization rates within the Martian nightside ionosphere.

Withers et al. [2012] analyzed 37 electron density profiles obtained by the Mars Express Radio Science Experiment (MaRS) for SZA 101°–123° and concluded that profiles for SZA < 115° showed trends consistent with the transport of dayside plasma. Above 115°, these profiles were consistent with simulated plasma production by electron precipitation. A review of previous modeling efforts concluded that spatial variations in precipitating electron populations appear sufficient to account for the observed patchiness of the nightside ionosphere.

2. Data and Instrument Overview

The Mars Atmosphere and Volatile EvolutioN mission (MAVEN) entered Mars orbit on 22 September 2014 UTC. MAVEN is designed to study the upper atmosphere of Mars and as such carries a full suite of instrumentation that allows it to measure the magnetic, electric, neutral, charged particle, and EUV environment [*Jakosky et al.*, 2015]. MAVEN is in an elliptical orbit about Mars with a periapsis of ~ 150 km, apoapsis of ~ 6000 km, and orbit period of ~ 4.5 h. The orbit precesses about Mars such that all local times (LT) will eventually be observed, allowing in situ measurements of all of the key plasma regions at Mars on the dayside and nightside.

The Langmuir Probe and Waves (LPW) instrument on board MAVEN consists of two cylindrical Langmuir Probes, each at the end of a ~ 7 m boom positioned on opposite sides of the main spacecraft body and separated by an angular distance of ~ 110°. The instrument measures several quantities, and for this study we focus on the results from the Langmuir Probe (LP) current-voltage (IV) sweeps [*Andersson et al.*, 2015].

During one LP subcycle, the LPW instrument measures one IV curve from one of the probes, from which various plasma properties can be derived, including electron density (Ne), electron temperature (Te), and spacecraft potential [see, for example, *Mott-Smith and Langmuir*, 1926; *Allen*, 1992; *Brace*, 1998]. A voltage is applied to one of the probes (1 or 2) and the resulting current to that probe measured. The voltage is sequentially stepped through 128 values, with the corresponding current measured at each step. The LPW fitting method is described in detail by *Andersson et al.* [2015] and *Ergun et al.* [2015]. Densities as low as ~100 cm^{-3} are measurable by LPW, which were not detectable by any previous remote sensing measurements. Currently, electron temperatures derived from the LPW instrument are thought to represent an upper limit to Te due to sensor surface material characteristics and atomic oxygen surface contamination of the probes, particularly at Te below ~ 0.15 eV (1650 K). This should be taken into account for the remainder of this study, and the reader is directed to *Ergun et al.* [2015] for more information.

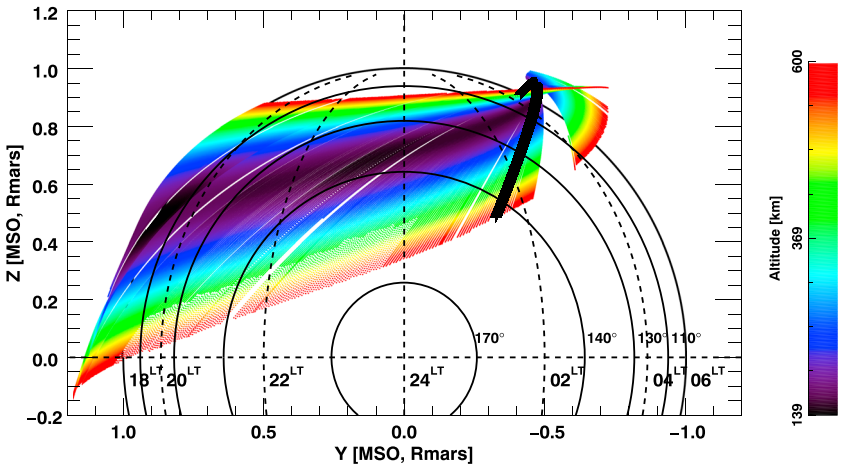

Figure 1. MAVEN orbit coverage for November 2014 through February 2015 in the MSO coordinate frame for altitudes below 600 km. Color represents altitude in kilometers. Curved dashed lines represent the labeled local times as projected onto the *Y*-*Z* plane. Solid curved lines represent SZA as projected onto the *Y*-*Z* plane. The direction of travel for any individual orbit is in the +*Z* direction. The thick black line represents the orbit track corresponding to the electron density and temperature profiles shown in Figure 2.

The data analyzed in this study span a time range of October 2014 through May 2015. MAVEN periapsis sampled the nightside of Mars during the months of approximately November 2014 through February 2015 with higher altitude measurements obtained on the nightside several months on either side of this. MAVEN has not yet sampled the dayside extensively, and these data are omitted for a later study once available. A case study of dayside electron density and temperature profiles is, however, available in *Ergun et al.* [2015].

For this study local time is referenced with respect to the Mars Solar Orbital (MSO) coordinate frame. We define noon (12 LT) as pointing directly from the center of Mars to the Sun; midnight (24 LT) is opposite to this. Dusk (18 LT) is in the positive *Y* MSO direction; dawn (6 LT) is in the negative *Y* MSO direction. The Sun is the main driver of the Martian ionosphere making the MSO reference frame appropriate for this study. LT was used instead of SZA because SZA will divide data up using concentric rings as projected onto the planet. The lack of solar driving on the nightside means we may expect to see dawn-dusk asymmetries, which will average out when binned by SZA. It should be noted that the *Z* direction in the MSO frame is offset from the planet rotation axis by ~24°.

We define nightside to lie between 18 LT through midnight and 6 LT and select all data for positive latitudes (i.e., the northern hemisphere, in MSO coordinates) within this range for altitudes below 600 km. Orbit coverage below 600 km for November through February is shown in Figure 1, where color represents altitude. Inbound orbits are to the south side of all periapses, outbound to the north. Because all observations within this study lie in the northern hemisphere, we assume that effects from crustal magnetic fields are small and are neglected here [e.g., *Acuña et al.*, 2001]. At an altitude of 120 km the Sun does not set until an SZA of approximately 105°, which is equivalent to ~19 LT. Hence, this study spans both the "twilight" and nightside ionosphere.

After the removal of unreliable sweeps the data set consists of just over 87,000 individual IV sweeps. Extreme spacecraft charging and cases where the automated fitting software could not obtain reliable fit values constituted unreliable sweeps. Further, the data were "filtered" so that only the most confidently fitted values are presented here. These have been binned into 12 bins of 1 h length and 10 (20) km altitude bins for electron density (temperature).

3. Electron Density and Temperature Observations

3.1. Individual Orbit Profiles

An example of the electron density and temperature profiles from one nightside periapsis pass that occurred at the dawn terminator between 22:09 UTC on 2 December 2014 and 22:32 UTC on 2 December 2014 is presented in Figure 2. The blue line represents the inbound part of the orbit and is on the nightside; red represents the outbound and is on the dayside. MAVEN approached periapsis from the southern magnetotail,

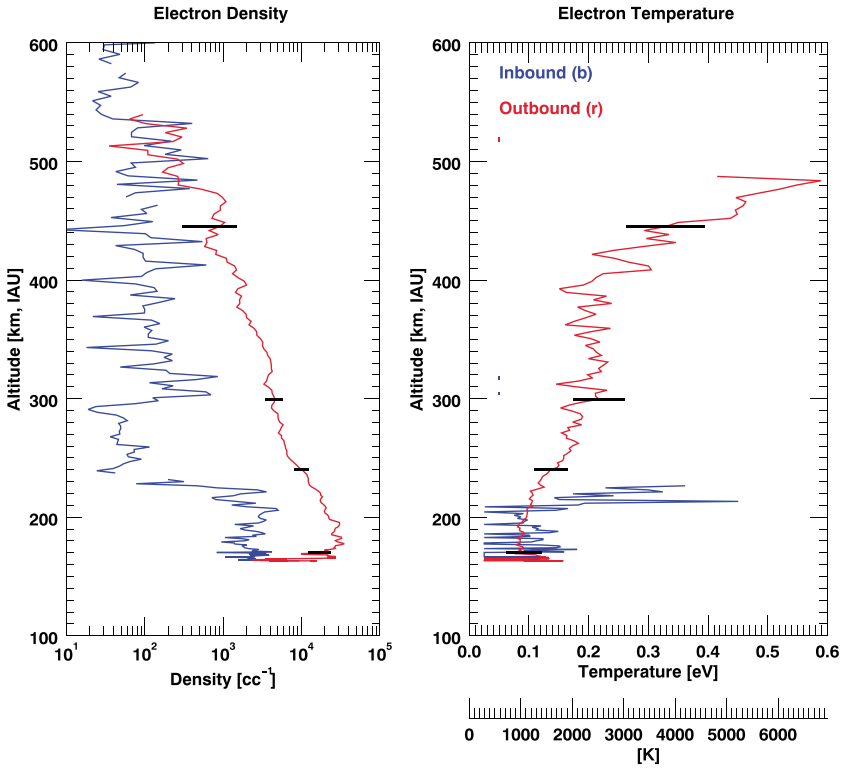

Figure 2. Altitude profiles of (left) electron density and (right) electron temperature for one periapsis pass between 22:09 UTC on 2 December 2014 at and 22:32 UTC on 2 December 2014. The dawn terminator was approximately at periapsis. The inbound portion of the orbit is colored blue and is on the nightside. The outbound portion is colored red and is on the dayside. Representative error bars are shown as black horizontal lines. Altitude is calculated in the Mars IAU frame, which is referenced to the IAU 2000 Mars Areodetic ellipsoid. (The origin is at the center of Mars, and the frame rotates with the solid body. X points from the center of Mars to 0° East longitude, 0° latitude. Y points from the center of Mars to +90° East longitude, 0° latitude. Z completes to the right-handed set.) Reduced signal-to-noise ratios below densities of ~200 cm^{-3} result in LP temperature measurement errors increasing to 100% or more, and therefore, such temperature measurements are omitted here.

crossing into the northern hemisphere before reaching periapsis. Periapsis was approximately at the dawn terminator, and the outbound leg of the orbit was close to the north pole on the dusk side of Mars in sunlight. This orbit has been highlighted in Figure 1 by the thick black line. The nightside profile shows large variability and dynamic behavior with electron densities 2 to 3 orders of magnitude lower than the dayside in this example. Representative error bars are shown at several altitudes by horizontal black lines.

3.2. Statistical Profiles

The nightside median electron density and electron temperature profiles binned as functions of altitude and local time as described earlier are presented in Figure 3 (left and right). Each line represents the median electron density or temperature for a certain local time, which is denoted by the line color. Dark red corresponds to 18 LT and is at dusk. Progressively lighter reds represent increasing LT, up to midnight (24 LT). Blue colors represent the dawn side, with light to dark blues representing 1 to 6 LT.

The electron density below ~200 km statistically increases with decreasing altitude, with peaks in electron density of ~3×10^3 cm^{-3} or greater observed between 150 and 180 km for 18, 19, and 6 LT. These are most likely sunlit peaks and a result of EUV photoionization, although plasma transport across the terminator may play a role as well. This density altitude trend is not necessarily the case for individual orbits as shown in Figure 2. Above ~200 km, the statistically observed electron densities follow an almost vertical profile. Individual orbits show that above ~200 km, significant structures and "blobs" of enhanced density over small altitude ranges are observed. The statistical result demonstrates that these structures and "blobs" do not appear to have any altitude dependencies.

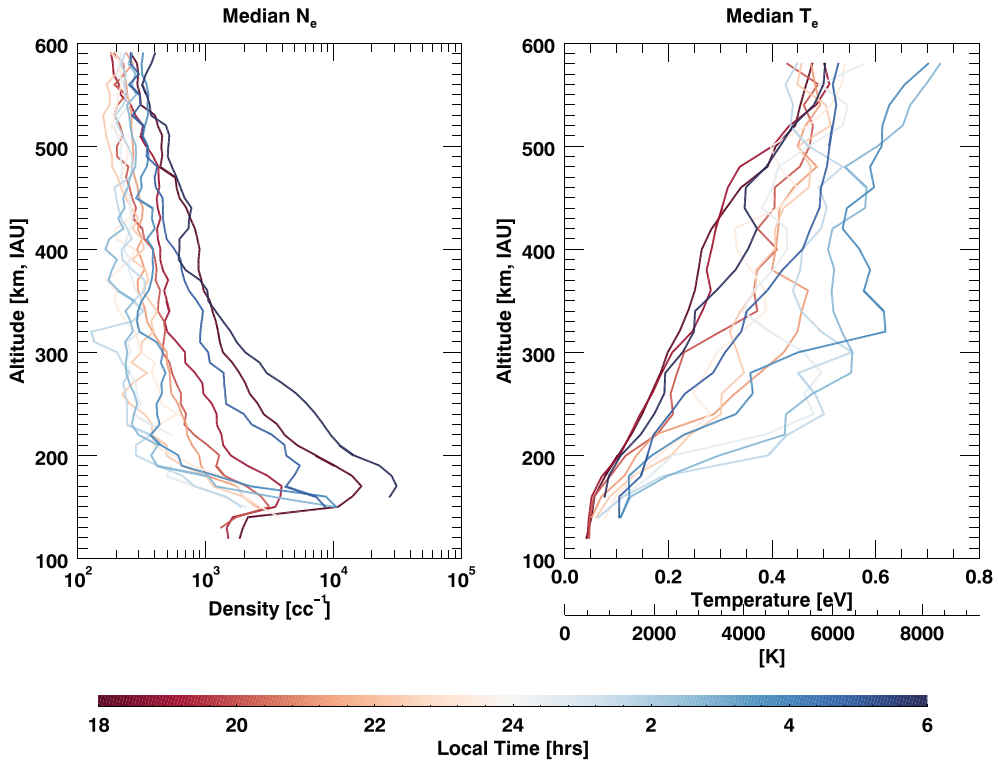

Figure 3. Statistical median altitude profiles of (left) electron density and (right) electron temperature. Both binned as described in the text. A local time of 18 corresponds to dusk, 24 to midnight, and 6 to dawn.

At local times of 18 LT to approximately midnight the electron density decreases due to the lack of solar EUV and the effect of recombination. The lowest densities are observed just after midnight at local times of approximately 1–2 LT. After ~2 LT electron density starts to increase again. At 6 LT the peak electron density is ~2×10^4 cm^{-3}, slightly larger than that at 18 LT. Due to the MAVEN orbit, observations made at dawn are at higher latitudes and closer to the pole than those made at dusk. Differences in terminator flow at the pole versus mid latitudes may contribute to the observed profile differences at 18 and 6 LT.

At high altitudes (>200–300 km) where the density is low ($\lesssim$1000 cm^{-3}), temperature increases ($\gtrsim$0.15 eV (1650 K)). The warmest temperatures are ~0.7 eV (7700 K) and are observed at ~2–3 LT above ~400 km. The lowest temperatures (< 0.15 eV (1650 K)) are observed below 200 km. Given that below Te ~0.15 eV (1650 K), the LPW Te measurement is an upper limit; these temperatures could be as low as the expected neutral temperature of 200–300 K (~0.02 eV) [*Nier and McElroy*, 1977]. An asymmetry between dawn and dusk temperatures exists for 19 < LT < 5, with dawn temperatures being approximately 1.5–2 times warmer than at dusk.

4. Discussion and Modeling Effort

The dayside ionosphere is sustained primarily by the photoionization of neutral atoms by EUV sunlight [e.g., *Chapman*, 1931a, 1931b; *Nagy et al.*, 2004; *Witasse et al.*, 2008; *Withers*, 2009]. This is naturally not the case on the nightside, and the rapid recombination of the ionospheric ions with free electrons rapidly reduces the densities of both. Analysis of ion composition from the Neutral Gass and Ion Mass Spectrometer (NGIMS) instrument on board MAVEN shows that for 45° < SZA < 60° O_2^+ is the dominant ion below ~300 km and that CO_2^+ is the second dominant ion below ~220 km. Above 300 km, O^+ is the dominant ion [*Withers et al.*, 2015]. We assume that these profiles are constant up to SZA 90° (dusk) at which point we assume the ionosphere is no longer driven by solar EUV and evolves as observed in the LPW data. In Figure 4a we show a simple simulation of the rate at which the plasma density drops once production ceases, and as an example, initial O_2^+ or CO_2^+ densities of ~ 10^6 cm^{-3} are reduced to ~ 10^2 cm^{-3} after 12 h. We assume a purely O_2^+ or CO_2^+ ionosphere and that the electron density (Ne) is equal to the ion density (Ni) for each case. The recombination rate is given by Ne × Ni × ki. Recombination rate coefficients, ki, were taken from *Fox and Sung* [2001].

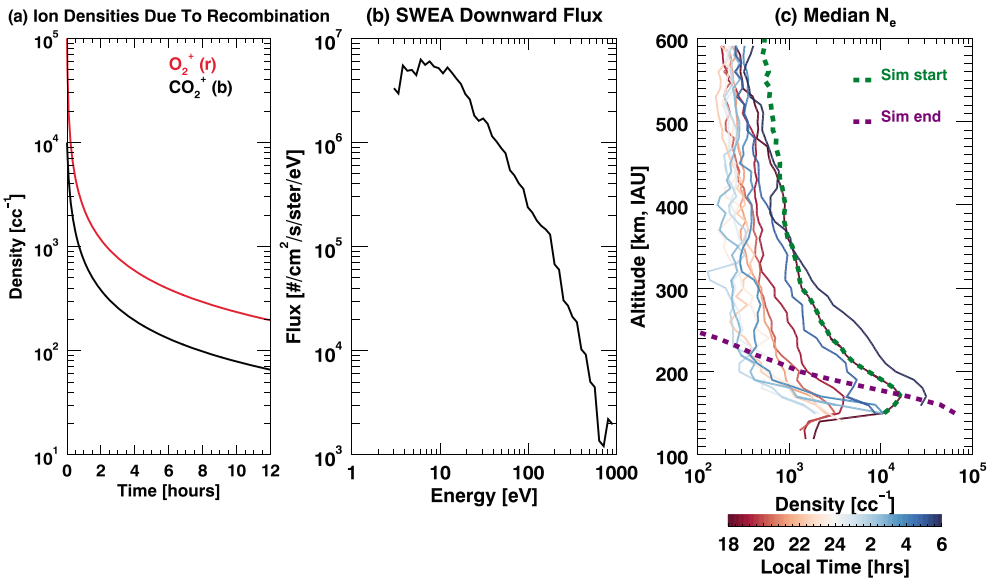

Figure 4. (a) Densities for O_2^+ and CO_2^+ ions based on recombination as a function of time. (b) Input spectrum for downward traveling precipitating electrons, as measured by SWEA at ~ 500 km at 05:11:59 UTC on 5 December 2014. (c) Median statistical electron densities as in Figure 3 with simulation results overplotted as dashed lines. Dashed green shows the input ion density profile; dashed purple shows the resulting equilibrium ion density profile that was obtained after ~25 min of run time. Precipitating electrons were included as calculated from the SWEA spectrum shown in Figure 4b.

Peak densities are observed between 150 and 180 km in Figure 3 (left), and here we simulate the ion density for this altitude range. An electron temperature of 300 K (0.02 eV) was hence assumed. The recombination rates for O_2^+ and CO_2^+ are inversely proportional to Te, and for comparison, an electron temperature of 1000 K (0.1 eV) resulted in densities of $\sim 5 \times 10^2$ cm^{-3} after 12 h.

The nightside ionospheric electron densities can have peak values of a few thousand cubic centimeter below ~ 200 km even for late local times as shown in Figure 3. Given that these densities are a factor of 10 or more greater than those expected from recombination alone as shown in Figure 4, there is a clear need for an additional ion source to sustain the nightside ionosphere. LPW has provided measurements of the low density ionosphere for the first time, and as such two possible source processes are evaluated in this study.

First, we assume quasi-neutrality and that the electron density loss at altitudes above 200 km, as the planet rotates, is returned to the ionosphere with a total ion density profile matching that of the electrons. Second, we assume an electron precipitation source. The Combined Atmospheric Photochemistry and Ion Tracing (CAPIT) 1-D photochemical model [*Andersson et al.*, 2010] was used to evaluate these possibilities within an assumed 45° magnetic field and a neutral collisionless atmosphere. The model solves key photochemical reactions for the major ion species (here O^+, O_2^+, CO_2^+, and N_2^+), with total initial ion density profiles matching those observed at 18 LT in Figure 3 (left).

4.1. Downward Flowing Ions

If all ions above 200 km were to flow downward into the ionosphere, could they sustain the ionosphere below this? O^+, O_2^+, and CO_2^+ are the dominant ion species, and as such each of three simulation runs assumed one of these ion species only with density profiles equal to the electron density profiles observed above 200 km at 18 LT in Figure 3. An infinite supply of downward flowing ions was available in the simulation that was able to charge exchange with neutrals via photochemical reactions to produce other ion species. We compare density profiles at 18 and 19 LT and assume that the density lost above ~ 200 km must travel on average 300 km downward to reach an altitude of 200 km over the course of 1 h. This constitutes a downward flow speed of ~ 80 ms^{-1}.

Downward flowing O_2^+ or CO_2^+ ions at 80 ms^{-1} were unable to sustain the observed densities below 200 km due to frequent collisions with the neutral atmosphere and recombination. Downward flow speeds

of 800 ms^{-1} could maintain a purely O_2^+ or CO_2^+ ionosphere at the density at which the infinite supply of ions enter the topside of the simulation. This flow speed is 10 times greater than the data suggest, and the resulting ionospheric composition is incorrect. Downward flowing O^+ ions at 80 ms^{-1} were able to sustain the observed densities; however, the resulting composition was incorrect, lacking any CO_2^+ ions. Due to these disagreements with NGIMS observations, we deem it unlikely that downward flowing ions play an important role in sustaining the nightside ionospheric densities observed below 200 km.

4.2. Precipitating Electrons

An ion source was included to represent ionization via precipitating electrons. An electron energy spectrum as measured by the Solar Wind Electron Analyzer (SWEA) instrument [*Jakosky et al.*, 2015] on MAVEN was used to produce ionization rate profiles as input to the CAPIT code. A representative nightside spectrum observed at ~500 km at 05:11:59 UTC on 5 December 2014 was used and is shown in Figure 4b. Pitch angle and energy distributions for downward flowing electrons as measured by SWEA were taken as inputs to the Mars Monte Carlo Electron Transport (MarMCET) model [*Lillis et al.*, 2009, 2011; *Lillis and Fang*, 2015] to derive the ionization rate profiles used in this study. The neutral atmosphere for the MarMCET model was taken from the Mars Global Ionosphere-Thermosphere Model [*Bougher et al.*, 2015] for equinox, equatorial, solar moderate conditions and is adequate for comparison purposes in this paper. Plasma transport processes were ignored.

The densities observed between ~ 19 and 5 LT below 200 km were sustainable (and at some LT greater than the observed densities) when precipitating electrons were included and simulation results are shown in Figure 4c. The dashed green line shows the initial total ion density profile for one simulation run which was chosen to match the observed electron density profile at 18 LT. The dashed purple line shows the equilibrium density profile of the simulation run, which is obtained after ~25 min. Below ~170 km, the simulation profile is greater than the observed densities by a factor of up to ~10, depending on LT. The cause of this is thought to be the use of a constant precipitating electron source within the simulation. SWEA observations show large dynamic variations in energy flux, and in some cases the observed spectra are sporadic in nature. As such, the constant precipitating source used here most likely causes an overestimate in the modeled nightside densities.

4.3. Electron Temperature

The anticorrelation between density and temperature is expected; at low altitudes the neutral and electron densities are high and collisions dominate, reducing the electron temperature to that of the neutral atmosphere. Above ~ 180 km, neutral densities decrease and collisions become less frequent. Electron temperature increases almost steadily above ~180 km suggesting that plasma processes dominate here, heating the electrons. Comparison to dayside temperature profiles close to the subsolar point in *Ergun et al.* [2015] shows that temperatures in the deep Martian tail (approximately $22 < LT < 4$) above ~ 300 km are greater than those on the dayside by factors of ~1.5 – 2. Current MAVEN coverage is limited, and it will be interesting to see if this is true for all nightside LT and latitudes at a later time in the mission.

5. Conclusions

The first nightside electron temperature profiles at Mars are presented as functions of altitude and local time. Particular focus in this study was given to the corresponding nightside electron density profiles, which are the first in situ electron density profiles to be measured on the nightside of Mars. The LPW instrument is able to resolve densities as low as ~100 cm^{-3} and observed the low density, dynamic behavior of the nightside ionosphere.

The observed electron densities below ~200 km are a factor of 10 or more greater than those expected if recombination alone were to act on the nightside of Mars and demonstrate the need for an ion source to maintain the nightside ionosphere. A collisionless version of the 1-D CAPIT code was used to investigate the effects of downward flowing ions and precipitating electrons to determine if either of these could maintain the observed ionosphere below 200 km. Downward flowing ion profiles were based on the observed electron densities after assuming quasi-neutrality. Ionization rates were calculated using the MarMCET code using measured electron energy spectra from the SWEA instrument on MAVEN.

Based on these simulations, downward flowing ions cannot sustain the ionosphere at the observed densities below 200 km due to frequent collisions with neutrals at these altitudes. Precipitating electrons appear to play an important role in sustaining the nightside ionosphere and were able to reproduce the observed nightside densities below 200 km. These latter findings are in agreement with previous conclusions drawn from analysis of earlier nightside data sets observed by previous missions at Mars.

Acknowledgments
Work at LASP and SSL was supported by NASA funding for the MAVEN project through the Mars Exploration Program. Work at IRF was supported by grants from the Swedish National Space Board (DNR 162/14) and Vetenskapsrådet (DNR 621-2014-5526). Data used in this study will shortly be available on the NASA Planetary Data System, via http://ppi.pds.nasa.gov/project/maven/lpw.html. This work was partially supported by the CNES for the part based on observations with the SWEA instrument embarked on MAVEN.

The Editor thanks two anonymous reviewers for their assistance in evaluating this paper.

References

Acuña, M., et al. (2001), Magnetic field of mars: Summary of results from the aerobraking and mapping orbits, *J. Geophys. Res.*, *106*(E10), 23,403–23,408.

Allen, J. (1992), Probe theory: The orbital motion approach, *Phys. Scr.*, *45*(5), 497.

Andersson, L., R. Ergun, and A. Stewart (2010), The combined atmospheric photochemistry and ion tracing code: Reproducing the viking lander results and initial outflow results, *Icarus*, *206*(1), 120–129.

Andersson, L., R. E. Ergun, G. T. Delory, A. Eriksson, J. Westfall, H. Reed, J. McCauly, D. Summers, and D. Meyers (2015), The Langmuir Probe and Waves (LPW) instrument for MAVEN, *Space. Sci. Rev.*, doi:10.1007/s11214-015-0194-3.

Bougher, S., D. Pawlowski, J. Bell, S. Nelli, T. McDunn, J. Murphy, M. Chizek, and A. Ridley (2015), Mars global ionosphere-thermosphere model: Solar cycle, seasonal, and diurnal variations of the mars upper atmosphere, *J. Geophys. Res. Planets*, *120*, 311–342, doi:10.1002/2014JE004715.

Brace, L. H. (1998), Langmuir probe measurements in the ionosphere, in *Measurement Techniques in Space Plasmas: Particles*, vol. 102, edited by R. F. Pfaff, J. E. Borovsky, and D. T. Young, pp. 23–36, AGU, Washington, D. C.

Chapman, S. (1931a), The absorption and dissociative or ionizing effect of monochromatic radiation in an atmosphere on a rotating earth, *Proc. Phys. Soc.*, *43*(1), 26–45.

Chapman, S. (1931b), The absorption and dissociative or ionizing effect of monochromatic radiation in an atmosphere on a rotating earth. Part II. grazing incidence, *Proc. Phys. Soc.*, *43*(5), 483–501.

Ergun, R. E., M. W. Morooka, L. Andersson, C. M. Fowler, G. T. Delory, D. J. Andrews, A. I. Eriksson, T. McEnulty, and B. M. Jakosky (2015), Dayside electron temperature and density profiles at Mars: First results from the MAVEN LPW instrument, *Geophys. Res. Lett.*, *42*, doi:10.1002/2015GL065280, in press.

Fjeldbo, G., A. Kliore, and B. Seidel (1970), The Mariner 1969 occultation measurements of the upper atmosphere of Mars, *Radio Sci.*, *5*(2), 381–386.

Fox, J. L. (1993), Upper limits to the nightside ionosphere of Mars, *Geophys. Res. Lett.*, *20*(13), 1339–1342.

Fox, J. L., and K. Sung (2001), Solar activity variations of the Venus thermosphere/ionosphere, *J. Geophys. Res.*, *106*(A10), 21,305–21,335.

Haider, S. (1997), Chemistry of the nightside ionosphere of Mars, *J. Geophys. Res.*, *102*(A1), 407–416.

Haider, S., J. Kim, A. Nagy, C. Keller, M. Verigin, K. Gringauz, N. Shutte, K. Szego, and P. Kiraly (1992), Calculated ionization rates, ion densities, and airglow emission rates due to precipitating electrons in the nightside ionosphere of Mars, *J. Geophys. Res.*, *97*(A7), 10,637–10,641.

Jakosky, B. M., et al. (2015), The Mars Atmosphere and Volatile EvolutioN (MAVEN) Mission, *Space Sci. Rev.*, 1–46, doi:10.1007/s11214-015-0139-x.

Lillis, R. J., and X. Fang (2015), Electron impact ionization in the Martian atmosphere: Interplay between scattering and crustal magnetic field effects, *J. Geophys. Res. Planets*, *120*, 1332–1345, doi:10.1002/2015JE004841.

Lillis, R. J., M. O. Fillingim, L. M. Peticolas, D. A. Brain, R. P. Lin, and S. W. Bougher (2009), Nightside ionosphere of Mars: Modeling the effects of crustal magnetic fields and electron pitch angle distributions on electron impact ionization, *J. Geophys. Res.*, *114*, E11009, doi:10.1029/2009JE003379.

Lillis, R. J., M. O. Fillingim, and D. A. Brain (2011), Three-dimensional structure of the Martian nightside ionosphere: Predicted rates of impact ionization from Mars Global Surveyor magnetometer and electron reflectometer measurements of precipitating electrons, *J. Geophys. Res.*, *116*, A12317, doi:10.1029/2011JA016982.

Lindal, G. F., H. B. Hotz, D. N. Sweetnam, Z. Shippony, J. P. Brenkle, G. V. Hartsell, R. T. Spear, and W. H. Michael (1979), Viking radio occultation measurements of the atmosphere and topography of Mars: Data acquired during 1 Martian year of tracking, *J. Geophys. Res.*, *84*(B14), 8443–8456.

Mott-Smith, H. M., and I. Langmuir (1926), The theory of collectors in gaseous discharges, *Phys. Rev.*, *28*(4), 727–763.

Nagy, A. F., et al. (2004), The plasma environment of Mars, *Space Sci. Rev.*, *111*, 33–114.

Němec, F., D. Morgan, D. Gurnett, and F. Duru (2010), Nightside ionosphere of Mars: Radar soundings by the Mars Express spacecraft, *J. Geophys. Res.*, *115*, E12009, doi:10.1029/2010JE003663.

Nier, A., and M. B. McElroy (1977), Composition and structure of Mars' upper atmosphere: Results from the neutral mass spectrometers on Viking 1 and 2, *J. Geophys. Res.*, *82*(28), 4341–4349.

Savich, N. A., and V. A. Samovol (1976), The nighttime ionosphere of Mars from Mars 4 and Mars 5 dual-frequency radio occultation measurements, in *Space Research*, vol. 16, edited by M. J. Rycroft, pp. 1009–1011, COSPAR, Paris.

Verigin, M., K. Gringauz, N. Shutte, S. Haider, K. Szego, P. Kiraly, A. Nagy, and T. Gombosi (1991), On the possible source of the ionization in the nighttime Martian ionosphere: 1. Phobos 2 HARP electron spectrometer measurements, *J. Geophys. Res.*, *96*(A11), 19,307–19,313.

Witasse, O., T. Cravens, M. Mendillo, J. Moses, A. Kliore, A. Nagy, and T. Breus (2008), Solar system ionospheres, *Space Sci. Rev.*, *139*, 235–265.

Withers, P. (2009), A review of observed variability in the dayside ionosphere of Mars, *Adv. Space Res.*, *44*(3), 277–307.

Withers, P., M. Fillingim, R. Lillis, B. Häusler, D. Hinson, G. Tyler, M. Pätzold, K. Peter, S. Tellmann, and O. Witasse (2012), Observations of the nightside ionosphere of Mars by the Mars Express Radio Science Experiment (MaRS), *J. Geophys. Res.*, *117*, A12307, doi:10.1029/2012JA018185.

Withers, P., et al. (2015), Comparison of model predictions for the composition of the ionosphere of Mars to MAVEN NGIMS data, *Geophys. Res. Lett.*, *42*, doi:10.1002/2015GL065205.

Zhang, M., J. Luhmann, and A. Kliore (1990), An observational study of the nightside ionospheres of Mars and Venus with radio occultation methods, *J. Geophys. Res.*, *95*(A10), 17,095–17,102.